Temperature dependence of Raman scattering in GaMnN

L. L. Guo, Y. H. Zhang, and W. Z. Shen[a)]
Laboratory of Condensed Matter Spectroscopy and Opto-Electronic Physics, Department of Physics, Shanghai Jiao Tong University, 1954 Hua Shan Road, Shanghai 200030, People's Republic of China

(Received 31 July 2006; accepted 6 September 2006; published online 20 October 2006)

A detailed investigation of temperature-dependent Raman scattering has been carried out on ion-implanted GaMnN with different Mn doses. The observed frequency downshift and linewidth broadening with increasing temperature can be well described by a model taking into account the contributions of the thermal expansion and decay of optical phonons into two and three phonons of lower energy. The authors have demonstrated clear dependence of the phonon frequency, linewidth, and decay process on the Mn concentration in GaMnN, which is found to be closely related to the crystal structure. © *2006 American Institute of Physics*. [DOI: 10.1063/1.2364472]

Considerable attention has been recently paid to diluted magnetic semiconductors (DMS) for creating a class of "spintronic" semiconductor devices with unprecedented functionality.[1,2] As a candidate of DMS, GaMnN is a very promising material, since many groups have predicted theoretically[2] and validated experimentally[3,4] that the Curie temperature of GaMnN exceeds room temperature. There have been numerous reports[3–6] about the growth of single-phase GaMnN by a variety of methods, and accordingly, the magnetic characterization with emphasis on the origin of the ferromagnetic behavior in GaMnN.[4,7] Another crucial step towards the realization of GaMnN-based devices is to clearly understand the structural and optical properties. X-ray diffraction,[8,9] photoluminescence,[10] and optical transmission[9] have been carried out for the Mn incorporation within the GaN crystal and Mn-related characteristics of emission and band gap engineering in GaMnN.

Raman scattering, as a nondestructive and effective probe technique for studying the lattice vibration characteristics, has been widely employed for GaMnN.[5,11–14] Gebicki *et al.*[11] have presented typical Raman peaks related to the disorder-active modes in GaMnN and simply reported the temperature-dependent frequencies of major Raman bands without detailed analysis. Mn-related local vibration mode (LVM) around 590 cm^{-1} has been observed by Hashimoto *et al.*[12] and confirmed by Refs. 13 and 14. In comparison with the Raman peaks of GaN, Yu *et al.*[14] have attributed the observed redshift of the A_1 [longitudinal optical (LO)] peak in GaMnN to strain caused by defects and the broadened linewidth to the deterioration of crystal structure.

Since the lattice constants and crystal quality were found to depend on the Mn concentration,[8,9] we expect that the variation of Raman frequency and linewidth in GaMnN will be strongly related to the Mn content. Furthermore, the information of phonon decay is an essential aspect to understand the phonon behaviors. Extensive investigation has been carried out on GaN, indicating that the three-phonon process dominates in the decay of A_1 (LO) phonon.[15] The introduction of Mn in GaN will result in the modifications of the crystal lattice, which may breakdown the translational symmetry. What is the phonon decay characteristic in GaMnN and how is the decay process related with the Mn concentration are still open questions.

The studied GaMnN samples were fabricated through uniform implantation of different Mn doses on high-quality Si-doped hexagonal GaN thin films [with thickness of 3.8 μm on (0001) sapphire substrates] at a constant energy of 190 keV. We selected five Mn-implantation doses of 1×10^{16}, 3×10^{16}, 5×10^{16}, 7×10^{16}, and 9×10^{16} cm^{-2}, corresponding to about 1%, 3%, 5%, 7%, and 9% Mn concentration in the implanted GaMnN region, respectively. After implantation, rapid thermal annealing (RTA) was carried out at 900 °C for 1 min in a flowing N_2 atmosphere. The estimated depth of the implanted GaMnN layers was about 150 nm from the sample surface. Details of the growth procedures and structural analysis were given elsewhere.[9] Temperature-dependent Raman measurements from 83 to 578 K were performed on a Jobin Yvon LabRAM HR 800 UV micro-Raman system.

Figure 1(a) shows the Raman spectra of the GaN and RTA GaMnN samples with different Mn-implantation doses at 83 K. The curves were recorded in a backscattering geometry of $z(x,-z)$ configuration. The Raman scattering in GaN was excited by the 514.5 nm line of an Ar-ion laser, while a 325 nm line of a He–Cd laser has been employed for GaMnN samples in order to exclude the strong Raman signal from GaN layers. The large absorption coefficient at 325 nm (about 10^5 cm^{-1}) leads to a depth of penetration of 100 nm, which is less than the thickness of GaMnN layers (about 150 nm).[9] The sharp Raman peaks of GaN located at 568 and 734 cm^{-1} correspond to E_2(high) and A_1(LO) phonon modes, respectively, while the peak at 420 cm^{-1} comes from the sapphire substrate.[13] It is clear that, after Mn implantation, the peaks become broadened and some other Raman

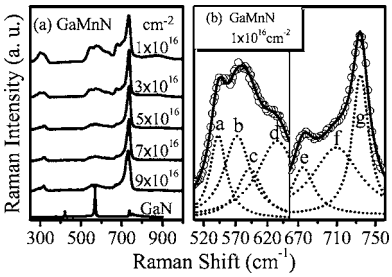

FIG. 1. (a) Raman spectra of GaMnN (including GaN) samples with different Mn-implantation doses at 83 K. (b) Raman spectra (open circles) of the GaMnN with Mn-implantation dose of 1×10^{16} cm^{-2}. The solid curve is the overall result of Lorentz fitting using seven Raman peaks (dotted curves), marked with a, b, c, d, e, f, and g.

[a)]Author to whom correspondence should be addressed; electronic mail: wzshen@sjtu.edu.cn

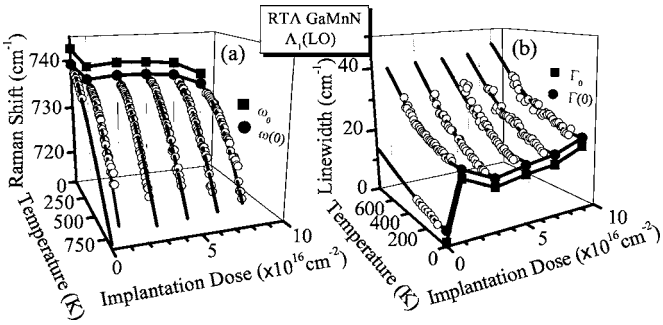

FIG. 2. Temperature-dependent (a) Raman frequency $\omega(T)$ and (b) Raman linewidth $\Gamma(T)$ of A_1(LO) mode (open circles), together with the theoretical fitting of Eqs. (1)–(3) (solid curves) for GaMnN samples (zero implantation dose corresponds to the unimplanted GaN sample). The solid circles represent (a) Raman frequency at 0 K [$\omega(0)$] and (b) Raman linewidth at 0 K [$\Gamma(0)$], while the solid squares show the values of (a) ω_0 and (b) Γ_0.

structures show up. To identify each of the contribution, we fit the observed Raman signal with Lorentz peaks based on the reported Raman peaks of GaMnN in the literature.

In Fig. 1(b), we take the sample with Mn-implantation dose of 1×10^{16} cm^{-2} as an example to fit the Raman spectrum. Seven peaks at about 545, 570, 585, 630, 670, 715, and 735 cm^{-1} are included in the fitting, which are marked with a, b, c, d, e, f, and g, respectively. Peaks b and g correspond to the E_2(high)- and A_1(LO)-phonon modes of GaMnN, with peaks d and f referred to as the disorder-active modes.[11] Harima[13] has assigned peak e to a LVM of GaN related to a vacancy, and peak c to be the LVM of Mn occupying the Ga site based on the GaN E_2(high) phonon. Similar analysis on this Mn-related LVM was also reported in Refs. 12 and 14. Though there is no observation of peak a in the literature, we can follow the identification of peak c for the origin of peak a. Since its frequency ($\sim$545 cm^{-1}) is close to a rough estimation based on the GaN A_1(TO)-phonon frequency consideration of the reduced-mass difference between the Ga–N and Mn–N pairs, i.e., $\omega_{\mathrm{Mn-N}}\sim\omega_{\mathrm{Ga-N}}[\mu_{\mathrm{Ga-N}}/\mu_{\mathrm{Mn-N}}]^{1/2}=547$ cm^{-1},[13] we can tentatively assign peak a to a LVM shifted from the A_1(TO) in GaMnN.

By the above Lorentz fitting processes, the temperature- and Mn-concentration-dependent phonon characteristics of frequency and linewidth could be obtained. It is found that these seven Raman modes have similar temperature dependence. We have also observed clear Mn concentration dependence of the E_2(high)-, A_1(LO)-phonon, and disorder-active modes, in contrast to the little change, as expected, of the LVM. In the following, we focus on the main optical phonon of A_1(LO) in GaMnN (peak g). Figure 2 shows the yielded temperature-dependent frequency and damping (open circles) of the zone-center optical phonon A_1(LO) of GaMnN. It is clear that the A_1(LO) structure shifts to lower frequency and broadens with increase of temperature. To model the yielded Raman shift, we can write the temperature-dependent Raman frequency $\omega(T)$ as[15,16]

$$\omega(T)=\omega_0+\Delta\omega_e(T)+\Delta\omega_s(T)+\Delta\omega_d(T), \tag{1}$$

with ω_0 the harmonic frequency of the optical mode and $\Delta\omega_e(T)$ the contribution of thermal expansion. Since the observed Raman signal is purely from the GaMnN layer under a 325 nm laser and the GaMnN layer is on the 3.8 μm thick GaN layer, $\Delta\omega_s(T)$ is the contribution from the lattice and thermal mismatch between the GaMnN and GaN layers.

TABLE I. Parameters for fitting the Raman frequency [Eqs. (1) and (2)] and linewidth [Eq. (3)] of GaN and RTA GaMnN samples.

Samples	Mn dose (%)	ω_0 (cm^{-1})	M_1 (cm^{-1})	M_2 (cm^{-1})	Γ_0 (cm^{-1})	N_1 (cm^{-1})	N_2 (cm^{-1})
GaN		742.5	2.80	0.15	1.10	3.27	0.17
RTA GaMnN ($\times10^{16}$ cm^{-2})	1	738.9	1.38	1.19	17.12	1.35	1.04
	3	739.2	2.09	0.68	12.70	2.68	0.86
	5	739.0	1.72	0.98	14.31	2.45	0.96
	7	738.5	1.49	1.11	15.29	1.67	1.20
	9	735.7	1.18	1.12	18.86	1.30	1.27

$\Delta\omega_e(T)$ and $\Delta\omega_s(T)$ can be calculated using the expression and parameters in Ref. 15. However, we assume that $\Delta\omega_s(T)=0$ in GaMnN sample since the lattice and thermal mismatches between GaMnN and GaN are negligible.

For the anharmonic coupling term $\Delta\omega_d(T)$ we can express it as

$$\begin{aligned}\Delta\omega_d(T)&=\Delta\omega_{d1}(T)+\Delta\omega_{d2}(T),\\ \Delta\omega_{d1}(T)&=M_1[1+n(T,\omega_1)+n(T,\omega_2)],\\ \Delta\omega_{d2}(T)&=M_2[1+3n(T,\omega_0/3)+3n^2(T,\omega_0/3)],\end{aligned} \tag{2}$$

with $n(T,\omega)=[\exp(\hbar\omega/k_BT)-1]^{-1}$. M_1 and M_2 are constants, which are selected as fitting parameters in the calculation. $\Delta\omega_{d1}(T)$ results from the decay of the zone-center phonons into two phonons (three-phonon process), where $\omega_1+\omega_2=\omega_0$ is unchanged, while $\Delta\omega_{d2}(T)$ represents the decay into three phonons (four-phonon process). For the case of GaN, the zone-center LO phonons cannot decay into two longitudinal acoustic or transverse acoustic phonons of equal frequency and opposite wave vector in the three-phonon process because $\omega_{\mathrm{LO}}>2\omega_{\mathrm{LA,TA}}$ over the whole phonon dispersion spectrum.[17] The possibility is to decay into two phonons with frequency $\omega_1\sim590$ cm^{-1} and $\omega_2\sim150$ cm^{-1},[18] which can be obtained from the phonon dispersion curves of GaN in Ref. 17. In the four-phonon process, we only consider the symmetric decay with frequency $\omega_0/3$,[16] since these decay channels can be easily found for A_1(LO) in the GaN phonon dispersion spectrum.

Phonon damping mainly arises from the decay into phonons with lower energies. Similar to the temperature dependency of Raman shift, the damping can be calculated by assuming again the asymmetric decay into two phonons and symmetric decay into three phonons[15,16] as follows:

$$\begin{aligned}\Gamma(T)&=\Gamma_0+\Gamma_1+\Gamma_2,\\ \Gamma_1&=N_1[1+n(T,\omega_1)+n(T,\omega_2)],\\ \Gamma_2&=N_2[1+3n(T,\omega_0/3)+3n^2(T,\omega_0/3)],\end{aligned} \tag{3}$$

with Γ_0 a damping contribution due to defect or impurity scattering, N_1 and N_2 are constants, Γ_1 is the damping part induced by the asymmetric decay of the three-phonon process, while Γ_2 represents the four-phonon process.

Figure 2(a) displays the theoretical fitting of Eqs. (1) and (2) solid curves with the fitting parameters ω_0, M_1, and M_2 listed in Table I to the temperature-dependent Raman frequencies $\omega(T)$ of the A_1(LO) mode in GaMnN (open circles). We note that the current model can describe well the

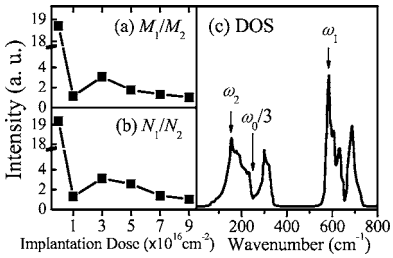

FIG. 3. Dependence of (a) M_1/M_2 and (b) N_1/N_2 on the Mn-implantation dose in GaMnN (including GaN) samples. (c) Calculated phonon density of states in GaN, with the positions of ω_1, ω_2, and $\omega_0/3$ marked.

downshift of the phonon frequency with increasing temperature. The harmonic frequency ω_0 and Raman frequency at 0 K $[\omega(0)]$ of the A_1(LO) mode have also been shown in Fig. 2(a) as solid squares and circles, respectively. It is seen that both of them have similar dependence on Mn-implantation dose. In addition to a small redshift in the Raman frequency (compared with that of GaN) of all these GaMnN samples, as reported in Ref. 14, we can clearly observe the variation of ω_0 with Mn-implantation dose, which can be attributed well to the change of the lattice constant. The overall increase of the lattice constant due to the Mn implantation corresponds well to the decrease of ω_0. Due to the incorporation of Mn substitutionally on the Ga sublattice at low Mn doses, the lattice constant decreases with the increase of Mn dose, resulting in the increase of ω_0. However, the lattice constant turns to increase as the Mn dose gained goes beyond 3×10^{16} cm^{-2}, which is due to the incorporation of interstitial Mn,[9] corresponding to the decrease of ω_0. The present Raman study also reveals that the highest implantation dose (concentration) for Mn substitution on the Ga sublattice is about 3×10^{16} cm^{-2} (3%), in good agreement with the x-ray diffraction observation.[8,9]

Figure 2(b) shows the least-squares fit of Eq. (3) (solid curves with fitting parameters Γ_0, N_1, and N_2 listed in Table I) to the experimental temperature-dependent linewidths $\Gamma(T)$ of the A_1(LO) mode in GaMnN (open circles). The values of Γ_0 and Raman linewidth at 0 K $[\Gamma(0)]$ of different Mn-implantation doses have also been shown as solid squares and circles, respectively. Again, both of Γ_0 and $\Gamma(0)$ have similar variation laws with increase of Mn-implantation dose. It can be clearly seen that there is a rapid increase in Γ_0 between GaMnN and GaN due to the formation of lattice defect and structural disorder after Mn implantation. Furthermore, the dependence of Γ_0 on the Mn-implantation dose also displays the closely related behavior with that of Urbach bandtail.[9] In the GaMnN samples, the replacement of Mn with Ga site at low Mn doses will release the structural disorder, resulting in the decrease of Γ_0, in contrast to the interstitial Mn case where the reverse effect occurs.

From the ratios of M_1/M_2 and N_1/N_2, the relative contributions of the three-phonon and four-phonon processes to the total phonon decay can be estimated. Figure 3 shows the ratios (a) M_1/M_2 and (b) N_1/N_2 for the A_1(LO) phonon of GaN and GaMnN samples. The variation of N_1/N_2 is very close to that of M_1/M_2, confirming the reliability of our results obtained from the theoretical fitting of the A_1(LO) phonon. For GaN, M_1/M_2 and N_1/N_2 are as high as ~20, indicating that the decay into two phonons is the prevailing process, while the four-phonon process makes minor contribution in the anharmonic coupling of the A_1(LO) phonon. This phenomenon has been reported in similar studies for GaN (Ref. 15) and proven to be consistent with the calculated phonon dispersion spectrum.[17] However, for the GaMnN samples, M_1/M_2 and N_1/N_2 are much smaller than those of GaN, indicating that the three-phonon process is drastically reduced while the probability of four-phonon one increases after Mn implantation.

We attribute the change of M_1/M_2 and N_1/N_2 to the observed fluctuation of ω_0 in Fig. 2(a) with by the aid of the calculated phonon density of states (DOS) of pure GaN (Ref. 17) shown in Fig. 3(c), where the positions of ω_1, ω_2, and $\omega_0/3$ have been marked. Compared with GaN, the decrease of ω_0 will cause smaller values of ω_1, ω_2, and $\omega_0/3$ in GaMnN accordingly. As shown above, the implantation of Mn in GaN causes lattice defect and structural disorder which break down the translational symmetry of GaN. In addition to the Brillouin zone center phonons, the phonons at Brillouin zone edges can also contribute to the first-order Raman scattering. In this case, the Raman spectra of GaMnN will reflect the features of the GaN phonon DOS. Figure 3(c) clearly shows that the phonon DOS decreases rapidly with ω_1 and ω_2, resulting in the fast reduction of the contribution of the three-phonon process, whereas the redshift of $\omega_0/3$ will lead to an increase in DOS, providing more probability for the four-phonon process. Therefore, as shown in Figs. 3(a) and 3(b), the values of M_1/M_2 and N_1/N_2 in GaMnN will be much smaller than those of GaN and the dependence of M_1/M_2 and N_1/N_2 on Mn-implantation dose, as expected, has a similar variation law to ω_0 displayed in Fig. 2(a).

This work was supported by the Natural Science Foundation of China, Shanghai Municipal Commission of Science and Technology, and the National Minister of Education Program for Changjiang Scholars and Innovative Research Team in University (PCSIRT).

[1] H. Ohno, Science **281**, 951 (1998).
[2] T. Dietl, H. Ohno, F. Matsukura, J. Cibert, and D. Ferrand, Science **287**, 1019 (2000).
[3] G. T. Thaler, M. E. Overberg, B. Gila, R. Frazier, C. R. Abernathy, S. J. Pearton, J. S. Lee, S. Y. Lee, Y. D. Park, Z. G. Khim, J. Kim, and F. Ren, Appl. Phys. Lett. **80**, 3964 (2002).
[4] M. J. Reed, F. E. Arkun, E. A. Berkman, N. A. Elmasry, J. Zavada, M. O. Luen, M. L. Reed, and S. M. Bedair, Appl. Phys. Lett. **86**, 102504 (2005).
[5] M. Zajac, R. Doradziński, J. Gosk, J. Szczytko, M. Lefeld-Sosnowska, M. Kamińska, A. Twardowski, M. Palczewska, E. Grzanka, and W. Gebicki, Appl. Phys. Lett. **78**, 1276 (2001).
[6] J. M. Baik, H. S. Kim, C. G. Park, and J. L. Lee, Appl. Phys. Lett. **83**, 2632 (2003).
[7] L. Kronik, M. Jain, and J. R. Chelikowsky, Phys. Rev. B **66**, 041203 (2002).
[8] G. Thaler, R. Frazier, B. Gila, J. Stapleton, M. Davidson, C. R. Abernathy, S. J. Pearton, and C. Segre, Appl. Phys. Lett. **84**, 1314 (2004).
[9] L. L. Guo, W. Z. Shen, and Y. H. Zhang, J. Appl. Phys. **99**, 113533 (2006).
[10] Y. Shon, Y. H. Kwon, T. W. Kang, X. Fan, D. Fu, and Y. Kim, J. Cryst. Growth **245**, 193 (2002).
[11] W. Gebicki, J. Strzeszewski, G. Kamler, T. Szyszko, and S. Podsiadlo, Appl. Phys. Lett. **76**, 3870 (2000).
[12] M. Hashimoto, Y. K. Zhou, H. Tampo, M. Kanamura, and H. Asahi, J. Cryst. Growth **252**, 499 (2003).
[13] H. Harima, J. Phys.: Condens. Matter **16**, S5653 (2004).
[14] Y. Y. Yu, R. Zhang, X. Q. Xiu, Z. L. Xie, H. Q. Yu, Y. Shi, B. Shen, S. L. Gu, and Y. D. Zheng, J. Cryst. Growth **269**, 270 (2004).
[15] A. Link, K. Bitzer, W. Limmer, R. Sauer, C. Kirchner, V. Schwegler, M. Kamp, D. G. Ebling, and K. W. Benz, J. Appl. Phys. **86**, 6256 (1999).
[16] X. D. Pu, J. Chen, W. Z. Shen, H. Ogawa, and Q. X. Guo, J. Appl. Phys. **98**, 033527 (2005).
[17] C. Bungaro, K. Rapcewicz, and J. Bernholc, Phys. Rev. B **61**, 6720 (2000).
[18] L. Shi, F. A. Ponce, and J. Menéndeza, Appl. Phys. Lett. **84**, 3471 (2004).